Eur. Phys. J. D **43**, 247–250 (2007)
DOI: 10.1140/epjd/e2007-00115-8

THE EUROPEAN PHYSICAL JOURNAL D

Embedding atom-jellium model for metal surface

L.-L. Wang[1,2] and H.-P. Cheng[1,a]

[1] Department of Physics and Quantum Theory Project, University of Florida, Gainesville, FL 32611, USA
[2] Department of Materials Science and Engineering, and the Frederick Seitz Materials Research Laboratory, University of Illinois at Urbana-Champaign, Urbana, IL 61801, USA

Received 13 August 2006 / Received in final form 13 October 2006
Published online 24 May 2007 –

Abstract. To describe metal surfaces efficiently and accurately, an embedding atom-jellium model is proposed. Within density functional theory, we consider a multiscale scheme that combines jellium and atomistic approaches. We use the former to model layers deep inside a metal surface to reduce the computational cost and the later to maintain the accuracy required for chemical bonding. Work functions of Al(111) and Cu(111) surfaces are studied using this model with comparisons to all-atom and pure jellium models. The much closer results of the embedding atom-jellium model to the all-atom results than to the pure jellium results show a good prospect for our approach in large-scale density functional calculations.

PACS. 71.15.Dx Computational methodology (Brillouin zone sampling, iterative diagonalization, pseudopotential construction) – 73.21.Ac Multilayers – 73.30.+y Surface double layers, Schottky barriers, and work functions

1 Introduction

The use of jellium to model metal dates back to Drude's work on conductivity. In the jellium model, nuclei and core electrons are replaced by a uniform positive background. Valence electrons move quantum mechanically in the field of this positive background. Bardeen [1] demonstrated that jellium is the simplest model to calculate electronic structure of metal surfaces, and Lang and Kohn [2,3] were the first to do self-consistent calculation using jellium to study the properties of metal surfaces within density functional theory (DFT) [4,5].

During the past decade, with developments in pseudopotentials, iterative minimization algorithms and computer hardware, accurate DFT calculations treating metal surfaces in a slab model, in which all metal atoms are described by pseudopotentials, have become routine [6], and the less accurate jellium model of metal surfaces seems outdated. However, on one hand, an all-atom calculation for the adsorption of a not-so-small molecule such as C_{60} and/or organic molecules on metal surfaces is already pushing the limit of today's computation capacity [7,8]. On the other hand, qualitatively correct results have been obtained by treating metal surface as a jellium for various adsorption systems, from H [9] and H_2O [10] to thin films [11]. The jellium model still has its advantage of numerical simplicity and can be taken as the simplest pseudopotential.

Here, unlike previous studies of using jellium to model the whole metal surface in an adsorption system, we propose to combine the advantages of both atomic and jellium pseudopotentials in the spirit of multiscale modeling to study large molecule adsorption on metal surfaces. In our embedding atom-jellium (EAJ) approach, the most important interface region, which includes the adsorbate molecule and the top metal layers, is described with the accurate atomic pseudopotential. This region is embedded in a jellium matrix, which is far enough from the interface region that the jellium description is acceptable. In doing so, computational cost is lowered without losing accuracy, and long-range effect due to delocalized s-electrons can be included. In this paper, as the first step of implementing and validating the EAJ model, we study the work functions of Al(111) and Cu(111) surfaces using the EAJ model. We find that the EAJ model improves dramatically over the simple pure jellium slab and gives results very close to the all-atom results.

The paper is organized in the following manner: the formulism is presented first in the method section, which is followed by results and discussion of Al(111) and Cu(111). The last section contains the final conclusions.

2 Method: DFT formulism for embedding atom-jellium model

In the embedding atom-jellium model, the potential of metal ions in deep surface is described by a jellium slab

[a] e-mail: cheng@qtp.ufl.edu

and the top surface region by atomistic pseudopotentials. The positive ions in the jellium slab are replaced by a uniform positive background, which occupies a volume Ω_{jel} in the surface unit cell, as

$$n_{jel}(\mathbf{r}) = \begin{cases} n_+ & \text{for } \mathbf{r} \in \Omega_{jel} \\ 0 & \text{otherwise.} \end{cases} \quad (1)$$

The parameter n_+ corresponds to the average charge density of nuclei+core electrons in the metal. Each charge is distributed in an effective volume, $(4\pi/3)\, r_s^2$, where r_s is the Wigner-Seitz radius. For a fcc metal, assuming Z as the net charge of a nuclei-core electrons unit for each metal atom, there is a simple relation

$$\frac{1}{n_+} = \frac{4\pi}{3} r_s^2 = \frac{a^3}{4Z}, \quad (2)$$

where a is the lattice constant. A key element in our model is that Z can be different than the positive charge in a metal ion in the atomistic region. For example, only s-electrons are included explicitly as valence electrons in the jellium region but any combination of s-, p-, and d-electrons can be included in the atomistic region.

We use a plane wave basis set for wave functions of valence electrons and three-dimensional period boundary conditions. With valence electrons, ions and a jellium slab in the system, the ground state total energy functional in DFT is

$$\begin{aligned} E &= T_0[n(\mathbf{r})] + E_{xc}[n(\mathbf{r})] + E_{es}[n(\mathbf{r})] \\ &= \sum_{i,\mathbf{k}} w_{\mathbf{k}} f_{i,\mathbf{k}} \int d^3r \psi^*_{i,\mathbf{k}}(\mathbf{r}) \left(-\frac{\nabla^2}{2}\right) \psi_{i,\mathbf{k}}(\mathbf{r}) + E_{xc}[n(\mathbf{r})] \\ &+ E_H[n(\mathbf{r})] + E_{pp}[n(\mathbf{r})] + E_{ion-ion}(\{\mathbf{R}_I\}) \\ &+ E_{el-jel}[n(\mathbf{r}); n_+] + E_{ion-jel}(\{\mathbf{R}_I\}, n_+) + E_{jel-jel}(n_+). \end{aligned} \quad (3)$$

The only difference from the conventional DFT is the electrostatic energy E_{es}, which now includes contributions from the jellium slab. Among them, $E_{ion-jel}$ and $E_{jel-jel}$ are constants for a fixed geometric configuration because they are independent of electron density $n(r)$, but these two terms need to be included correctly in the total energy, which in turn will allow the correct calculation for Hellmann-Feynman force. The self-consistent Kohn-Sham equation is

$$\left(-\frac{\nabla^2}{2} + V_{xc}(\mathbf{r}) + V_H(\mathbf{r}) + V_{pp}(\mathbf{r}) + V_{jel}(\mathbf{r})\right) \psi_{i,\mathbf{k}}(\mathbf{r}) = \varepsilon_{i,\mathbf{k}} \psi_{i,\mathbf{k}}(\mathbf{r}), \quad (4)$$

where the jellium potential

$$V_{jel}(\mathbf{r}) = -\int d^3r' \frac{n_{jel}(\mathbf{r})}{|\mathbf{r} - \mathbf{r}'|} \quad (5)$$

describes the Coulomb interaction between the positive jellium slab and electrons.

Following the formulism of total energy calculation with three-dimensional PBC [12,13], we can cast the energy between electrons and jellium into reciprocal space as

$$\begin{aligned} E_{el-jel} &= -\int_\Omega d^3r\, n(\mathbf{r}) \int_\Omega d^3r'\, n_{jel}(\mathbf{r}') \left[\chi(\mathbf{r}, \mathbf{r}')\right]_{\eta\to\infty} \\ &= -\int_\Omega d^3r\, n(\mathbf{r}) \int_\Omega d^3r'\, n_{jel}(\mathbf{r}') \left(\frac{4\pi}{\Omega}\right) \\ &\quad \times \sum_{\mathbf{G}\neq 0} \frac{1}{|\mathbf{G}|^2} e^{i\mathbf{G}\cdot(\mathbf{r}-\mathbf{r}')} \\ &= -\left(\frac{4\pi}{\Omega}\right) \sum_{\mathbf{G}\neq 0} \frac{1}{|\mathbf{G}|^2} \int_\Omega d^3r\, n(\mathbf{r})\, e^{i\mathbf{G}\cdot\mathbf{r}} \\ &\quad \times \int_\Omega d^3r'\, n_{jel}(\mathbf{r}')\, e^{-i\mathbf{G}\cdot\mathbf{r}'} \\ &= -\Omega \sum_{\mathbf{G}\neq 0} \frac{4\pi}{|\mathbf{G}|^2} n^*(\mathbf{G})\, n_{jel}(\mathbf{G}) \\ &= -\Omega \sum_{\mathbf{G}\neq 0} V_{jel}(\mathbf{G})\, n^*(\mathbf{G}), \end{aligned} \quad (6)$$

where

$$V_{jel}(\mathbf{G}) = \frac{4\pi}{|\mathbf{G}|^2} n_{jel}(\mathbf{G}) \quad (7)$$

is the Fourier transform of the jellium potential $V_{jel}(\mathbf{r})$. Similarly, the energy between jellium and itself is

$$\begin{aligned} E_{jel-jel} &= \frac{1}{2} \int_\Omega d^3r\, n_{jel}(\mathbf{r}) \int_\Omega d^3r'\, n_{jel}(\mathbf{r}') \left[\chi(\mathbf{r}, \mathbf{r}')\right]_{\eta\to\infty} \\ &= \frac{\Omega}{2} \sum_{\mathbf{G}\neq 0} V_{jel}(\mathbf{G})\, n^*_{jel}(\mathbf{G}). \end{aligned} \quad (8)$$

Because the interaction between the ions and the jellium is also straightforward Columb repulsion, the energy between them can be expressed as

$$\begin{aligned} E_{ion-jel} &= \int_\Omega d^3r\, n_{jel}(\mathbf{r}) \int_\Omega d^3r' \\ &\quad \times \sum_I Z_I \delta(\mathbf{r}' - \mathbf{R}_I) \left[\chi(\mathbf{r}, \mathbf{r}')\right]_{\eta\to\infty} \\ &= \frac{4\pi}{\Omega} \sum_{\mathbf{G}\neq 0} \int_\Omega d^3r\, n_{jel}(\mathbf{r})\, e^{i\mathbf{G}\cdot\mathbf{r}} \frac{1}{|\mathbf{G}|^2} \\ &\quad \times \int_\Omega d^3r' \sum_I Z_I \delta(\mathbf{r}' - \mathbf{R}_I)\, e^{-i\mathbf{G}\cdot\mathbf{r}'} \\ &= \Omega \sum_{\mathbf{G}\neq 0} \frac{4\pi}{|\mathbf{G}|^2} S(\mathbf{G})\, n^*_{jel}(\mathbf{G}), \end{aligned} \quad (9)$$

where

$$S(\mathbf{G}) = \sum_I \left(\frac{Z_I}{\Omega}\right) e^{-i\mathbf{G}\cdot\mathbf{R}_I} \quad (10)$$

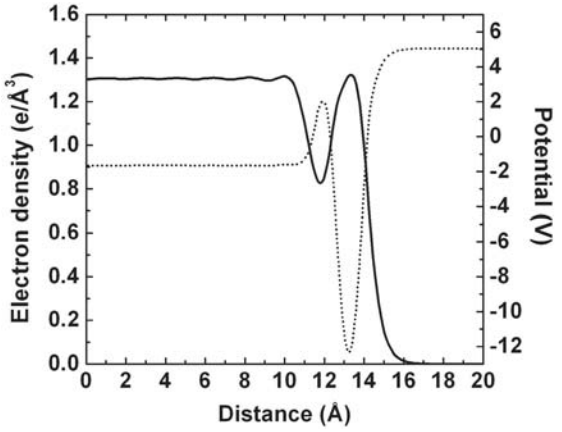

Fig. 1. The planar average electron density (solid) and potential (dotted) in the z-direction (perpendicular to the surface) for a 12-layer Al in EAJ model with 1-layer Al atom on each side of the 10-layer Al jellium. Only half of the supercell is shown.

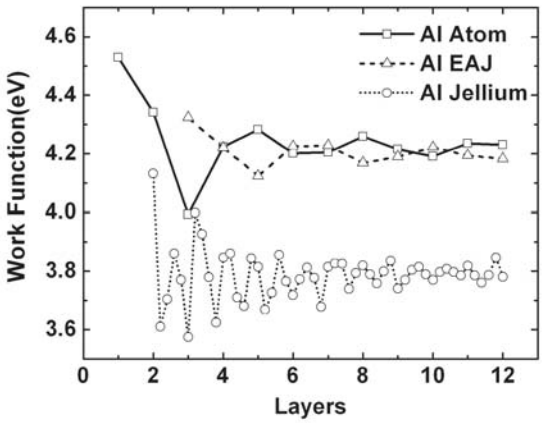

Fig. 2. Work function of Al surface as a function of the number of layers. Three different models are shown together: all atom (solid line with squares), EAJ (dashed line with triangles) and pure jellium (dotted line with circles).

is the structure factor of the ions. Finally, the force exerted on the ions by the jellium is

$$\mathbf{F}_{ion-jel}\left(\{\mathbf{R}_I\}\right) = -\frac{\partial E_{ion-jel}}{\partial \mathbf{R}_I} = i\Omega \sum_{\mathbf{G}\neq 0} \mathbf{G} \frac{4\pi}{|\mathbf{G}|^2} \left(\frac{Z_I}{\Omega} e^{-i\mathbf{G}\cdot\mathbf{R}_I}\right) n^*_{jel}\left(\mathbf{G}\right), \tag{11}$$

which will be added to other contributions from electrons and ions.

The EAJ model has been implemented in two popular packages of DFT total energy calculations using a plane-wave basis set, fhi98md [14] and VASP [15,16].

3 Results and discussion

To test whether EAJ model can describe well the properties of metal surfaces, we have studied the work functions of Al(111) and Cu(111) surfaces. Bulk Al and Cu both have fcc structure. We use an ultra-soft pseudopotential [17] for metal atoms. The DFT exchange-correlation functional we use is the local density approximation (LDA). With these choices, the lattice constant is 3.98 and 3.52 Å for fcc Al and Cu, respectively. The (111) surface has a hexagonal supercell with one atom in each layer. For this supercell, a Monkhorst-Pack [18] k-point mesh of $23 \times 23 \times 1$ with 56 irreducible points is found to be sufficient. The energy cutoff is 250 eV.

In Figure 1, the planar average electron density and total effective potential are plotted in the z-direction for a Al(111) surface, which is modeled by a 12-layer EAJ slab. The symmetric supercell consists of a 10-layer Al jellium with a 1-layer Al atom on each side of the jellium. The vacuum in the z-direction is about 15 Å to ensure a good calculation of work function for the surface. For the half of the supercell that is shown, the jellium edge is at $z = 11.5$ Å. The equilibrium distance between the Al atom and jellium is 1.65 Å, which is smaller than the interlayer distance of 2.30 Å for an all-atom Al(111) surface. The electron density fluctuates around the jellium edge. The amplitude of the fluctuation is reduced going to the center of the positive jellium background. This fluctuation has the characteristic of Friedel oscillations, as expected. These features correspond well with the total effective potential shown on the right in Figure 1.

Table 1. Work function (eV) of Al(111) and Cu(111) calculated in three different models.

	Atom	EAJ	Jellium
Al(111)	4.21	4.20	3.78
Cu(111)	5.24	5.17	3.55

To model a semi-infinite metal surface with a slab of finite thickness, the convergence of the properties with respect to the thickness, or the number of layers in the slab, needs to be checked because the properties of a metal thin film are subject to the quantum size effect (QSE) [19]. With more and more layers in the z-direction, the surface bands are shifted down to touch the Fermi level one by one. As the thickness of the slab increases, the gap between the surface bands decreases, and so does the oscillation in the QSE. The QSE of work function for Al(111) is shown in Figure 2 for three different slab models. The QSE for a pure jellium slab is the largest among the three slabs. The work function converges to 3.78 eV for a pure jellium Al slab, which is 0.4 eV smaller than the all-atom Al slab. As shown by the dashed line for EAJ model, if the top layer of jellium is replaced by an Al atom, the work function improves dramatically, in agreement with the all-atom result. The converged work functions are also listed in Table 1. The opposite trend of QSE for EAJ and all-atom model is due to the different symmetries of the slabs; for the EAJ slab, there is always a mirror plane at $z = 0$.

Although the work function for Al(111) can be described well by EAJ instead of all-atom model, it does

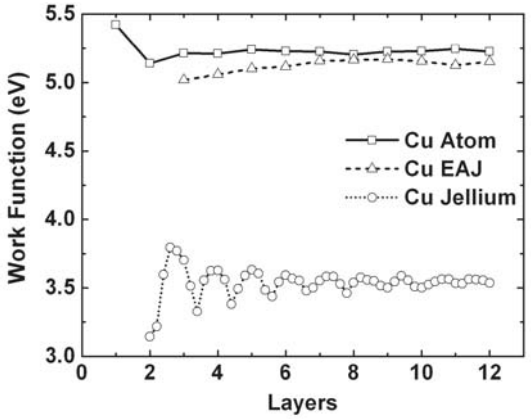

Fig. 3. Work function of Cu surface as a function of the number of layers. Three different models are shown together, all atom (solid line with squares), EAJ (dashed line with triangles) and pure jellium (dotted line with circles).

not reduce the computational cost because each Al jellium also has three valence electrons. To fulfill the motivation of using EAJ model to reduce the computational cost in a multi-scale sense, we study a Cu(111) surface. Cu has a filled valence d shell, so a Cu jellium has 10 fewer electrons than a Cu atom. In Figure 3, we show the results of the three slab models for a Cu(111) surface. The pure jellium model differs by 1.7 eV from the all-atom result, which demonstrates the importance of the contribution from d electrons. Our EAJ result of 5.17 eV compares favorably with the all-atom result of 5.24 eV (see Tab. 1). This shows that the work function of a surface is largely determined by the top layer. By replacing the deep layers with jellium with only one electron per site, a large computational cost has been saved and the work function is still described well. The saving comes from the reduction in the number of bands, which has a linear relation with the computational cost. For example, for a 7-layer slab, the CPU time for the EAJ model is only 40% of the all-atom model.

The physical mechanism for large improvement on work function by our EAJ model with respect to the simple jellium model is that the s electrons on the surface are now described realistically, as in the presence of the d and p electrons in the top layer. This is in the similar spirit that by including the lattice effect in the stabilized-jellium model [20–22], a better description of s electrons and thus work function can be achieved than the simple jellium model.

4 Conclusion

In conclusion, we have proposed and implemented the embedding atom-jellium (EAJ) model, combining jellium and atomic pseudopotentials, as a multiscale scheme to describe the properties of metal surfaces. We have shown that the work functions of Al(111) and Cu(111) can be well described in the EAJ model. The improvement of the work function for EAJ model over pure jellium model is dramatic for both simple metal Al with only sp electrons and noble metal Cu with filled d electrons. Studies of chemisorption with the EAJ model in large-scale density functional calculations are in progress.

This work was supported by DOE/Basic Energy Science/Computational Material Science under Contract No. DE-FG02-97ER45660.

References

1. J. Bardeen, Phys. Rev. **49**, 653 (1936)
2. N.D. Lang, Solid State Commun. **7**, 1047 (1969)
3. N.D. Lang, W. Kohn, Phys. Rev. B **3**, 1215 (1971)
4. P. Hohenberg, W. Kohn, Phys. Rev. B **136**, B864 (1964)
5. W. Kohn, L.J. Sham, Phys. Rev. **140**, 1133 (1965)
6. M.C. Payne, M.P. Teter, D.C. Allan, T.A. Arias, J.D. Joannopoulos, Rev. Mod. Phys. **64**, 1045 (1992)
7. W.L. Yang, V. Brouet, X.J. Zhou, H.J. Choi, S.G. Louie, M.L. Cohen, S.A. Kellar, P.V. Bogdanov, A. Lanzara, A. Goldoni, F. Parmigiani, Z. Hussain, Z.X. Shen, Science **300**, 303 (2003)
8. L.-L. Wang, H.-P. Cheng, Phys. Rev. B **69**, 045404 (2004)
9. O. Gunnarsson, B.I. Lundqvist, H. Hjelmberg, Phys. Rev. Lett. **37**, 292 (1976)
10. D.L. Price, J.W. Halley, Phys. Rev. B **38**, 9357 (1988)
11. E. Ogando, N. Zabala, E.V. Chulkov, M.J. Puska, Phys. Rev. B **71**, (2005)
12. G. Makov, M.C. Payne, Phys. Rev. B **51**, 4014 (1995)
13. J. Ihm, A. Zunger, M.L. Cohen, J. Phys. C-Solid State Phys. **12**, 4409 (1979)
14. M. Bockstedte, A. Kley, J. Neugebauer, M. Scheffler, Comp. Phys. Commun. **107**, 187 (1997)
15. G. Kresse, J. Furthmüller, Comput. Mat. Sci. **6**, 15 (1996)
16. G. Kresse, J. Furthmüller, Phys. Rev. B **54**, 11169 (1996)
17. D. Vanderbilt, Phys. Rev. B **41**, 7892 (1990)
18. H.J. Monkhorst, J.D. Pack, Phys. Rev. B **13**, 5188 (1976)
19. F.K. Schulte, Surf. Sci. **55**, 427 (1976)
20. N.W. Ashcroft, D.C. Langreth, Phys. Rev. **155**, 682 (1967)
21. R. Monnier, J.P. Perdew, Phys. Rev. B **17**, 2595 (1978)
22. A. Kiejna, Phys. Rev. B **43**, 14695 (1991)